

Secondary ion emission from frozen alkanes and benzene induced by MeV-ion impact

M. Wagner and K. Wien

Institut für Kernphysik der Technischen Hochschule Darmstadt, Darmstadt, Germany

B. Curdes and E.R. Hilf

Fachbereich Physik, Carl von Ossietzky Universität, Oldenburg, Germany

Received 13 November 1992 and in revised form 23 March 1993

Frozen samples of twelve alkanes and benzene were irradiated by ^{252}Cf fission fragments in order to study secondary ion emission by means of time-of-flight mass spectroscopy. The mass spectra are to a certain extent similar to electron-impact spectra of gaseous samples. The pattern of the negative ions could be assigned to dissociation after electron capture and frequent collisional reactions in the destruction zone of the nuclear track. Due to the substructure of the mass spectra we emphasize that the bonding type of the negative hydrocarbon ions is mostly acetylenic. The positive ion spectra strongly depend on the structure of the original molecules. They exhibit – contrary to the negative ion spectra – molecular ions, cluster ions and molecule-specific fragment ions. Model calculations were used to investigate the possible synthesis of carbon clusters inside an expanding plasma from the infratrack. For the ultratrack earlier molecular fragmentation calculations are supplemented by modelling the dehydration which is best fitted if assumed to take place subsequent to the fragmentation on a thermal time scale. The molecular cluster distributions are calculated by an explosive breakup model of sputtered material.

1. Introduction

PDMS is an abbreviation for plasma desorption mass spectrometry, an analytical method propagated by Macfarlane in 1974, when he and his co-workers discovered that nonvolatile molecules can be desorbed from solid organic material by ^{252}Cf fission fragments [38,51]. Their intuitive idea was that the ejection process is related to a plasma formed along the nuclear track shortly after the impact of the high energetic heavy ion. Meanwhile, the mass spectroscopic data of the ejecta – in particular the angular distributions of secondary ions [17,40] – have led to the conclusion that large intact molecules or molecular clusters are emitted not from the plasma, but from surface areas beside the inner track zone. Related desorption models suppose that the highly energized inner zone (infratrack) is a source for coherent atomic motion – i.e. a mechanical pressure pulse [29] or a shock wave [4] causing ablation at the surface. The charged ejecta of this type of processes generally form the high mass part of corresponding mass spectra – i.e. the molecular ions and certain molecule-specific fragment ions. They are characteristic for the sample material as well

as for its molecular structure. In the past, this part of the mass spectrum has been mainly used for PDMS.

So far, there exists only little experimental support of Macfarlane's original assumption, that the material close to the nuclear track becomes gaseous or even a plasma and expands into vacuum. PDMS experiments with Langmuir–Blodgett films have shown [43,45] that ions are ejected not only from the uppermost surface layer but also from layers as deep as 10 monolayers underneath the surface. The authors [45] supposed the formation of a crater, out of which the ejecta – molecular particles and destruction products – are blown into vacuum. Inspired by this suggestive picture, Moshhammer [40] tried to describe experimental energy and angular distributions of small fragment ions by a Maxwell distribution superposed on a gas flow into the direction of the heavy ions path. The temperature of this gas turned out to be about 10^4 K and its flow velocity about 2000 m/s. Due to this flux of particles in direction of the heavy ions path, the angular distribution of the secondary ions should be asymmetric with respect to the surface normal, when the angle of incidence is non-normal. Experiments on radial energy distributions of secondary ions performed by Fenyö et al. [19] proved, however, that for various angles of incidence the emission pattern of small fragment ions is symmetrical about the surface normal.

Correspondence to: M. Wagner, Institut für Kernphysik der Technischen Hochschule Darmstadt, Schlossgartenstrasse 9, W-6100 Darmstadt, Germany.

The aim of the present work was to obtain information about the desorption process by measuring the complete mass distribution of secondary ions ejected from simple organic compounds by fission fragments of ^{252}Cf . In case the highly energized zone around the nuclear track is transformed into a plasma, a certain fraction of the secondary ions should be associated to vigorous molecular destruction inside this plasma. In accordance to the degree of destruction, the fragmentary part of the spectra is then more or less independent from the original structure of the irradiated compound. These fragment ions should appear in the low mass region of the spectra, which so far has been of minor interest for mass spectroscopic purposes.

The main experimental problem was to produce clean samples and to avoid contamination of these samples during the measurement of time-of-flight (TOF) mass spectra. The low mass part of PDMS spectra is generally dominated by ions from volatile low mass contaminants being adsorbed to the sample surface from air or the residual gas in the vacuum system. The samples were generated by condensing an organic gas on a cold metal surface in vacuum. The TOF spectra were taken while blowing the gas onto the metal – that means, during continuous refreshment of the sample.

The patterns of the secondary ion mass spectra are compared with some model calculations. In a recent paper [28] we had considered the hydrodynamic expansion of the material of the innermost part of the track assumed to be an atomized gas studying its fast coagulation to clusters or molecular species. In the last section we study models assumed here to lead to the positive ion mass spectra. An assumed purely entropic (fast and cool) breakup and desorption of the total crater material gives best agreement to the experimental molecular cluster series. The assumed to be thermal (excited fragments, time scale long as compared to molecular vibration times) hydrogen detachment of the created molecular fragments thus well after the fast desorption seems to fit relatively best the experimental data.

2. Samples and the problem of rest gas adsorption

The most convenient sample material would have been graphite, which exhibits, however, only very small secondary ion yields under MeV-ion bombardment. Due to its high electrical conductivity, graphite is probably not affected by electronic sputtering.

The samples used in the present experiments were the following hydrocarbon compounds:

alkanes $\text{CH}_3-(\text{CH}_2)_n-\text{CH}_3$, $n = 1-12$,
benzene C_6H_6 .

These compounds are gaseous or liquid at room temperature. Their vapour was condensed onto a Cu surface at temperatures between -190 and -110°C . PD mass spectra of such frozen gases have been measured already in earlier experiments by us [55]. A Japanese group [50] has published secondary ion mass spectra of frozen C_2H_2 being irradiated by 1.25 MeV/n Ar ions. Both sets of spectra show several lines in the low mass regime, which cannot originate from hydrocarbon compounds. They appeared, for instance, at $m/z = 16$ (O^\pm), 17 (OH^-), 19 (H_3O^+), 23 (Na^+) and 26 (CN^-). In addition, the negative spectrum of decane shown in fig. 2 of ref. [55] contains a series of broad mass lines between $m = 135$ amu and $m = 698$ amu. This series was associated with cluster ions, but it turned out later, that we observed an electronic artefact due to oscillations of the very high secondary electron signal. The non-hydrocarbon lines are mainly produced by molecules adsorbed to the sample surface from the residual gas of the vacuum system. The measurements presented here were particularly disturbed by acetone ($M=58$ amu), which was used to clean parts of the vacuum chamber. The acetone had a partial pressure of less than 10^{-10} mbar and could be easily identified by pronounced mass lines at $(M\pm H)^\pm$ and the corresponding dimers.

Fig. 1 illustrates how the adsorbed rest gas builds up on the sample surface at a total pressure of 1×10^{-7} mbar inside the vacuum chamber. The target was a copper metal at the temperature of liquid nitrogen cleaned by Ar-ion etching. The growth of ion yields is characterized by two rise times, the first in the order of 2.5 min and the second in the order of several hours. The first rise time is obviously associated with the growth of the first monolayers. Complete coverage is indicated by the disappearance of the O^+ signal, which originates probably from copper oxide. The further growth of the ion rate is much slower and depends on the type of ion. For instance, the H_3O^+ signal (adsorbed water) steadily increases and does not reach saturation within 4 h. The heavier hydrocarbon ions tend to saturate later than the small ions. The fact that the ion yields increase even after a complete surface coverage, might be explainable by desorption from layers underneath the top layer or by the depth effect [56] – i.e. long range interaction out of the organic bulk material. One has to be aware that also the metallic substrate can influence ionization.

A second interesting observation is, that for heavier molecules the first ion signals occur after a distinct time gap. This gap seems to increase with the mass of the desorbed species. Molecular ions, which obtain their charge by protonation like the molecular ion of acetone or its dimer, need an organic neighbourhood. That means, a certain density of adsorbed rest gas molecules is required. Eventually, protonation is the

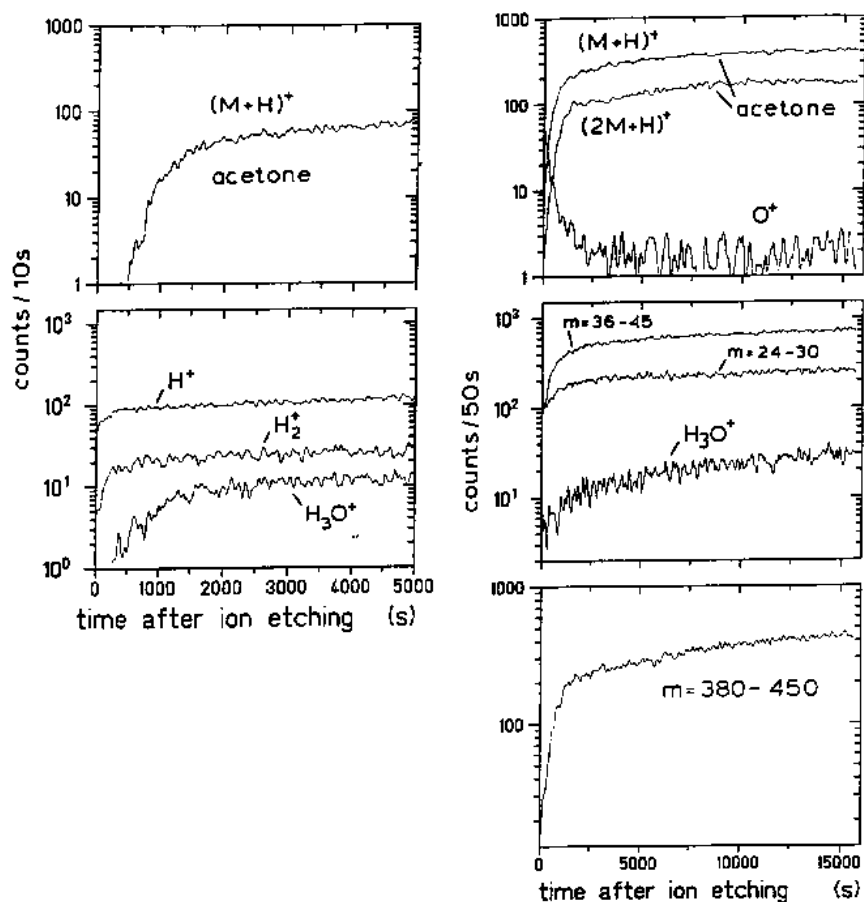


Fig. 1. Growth curves of material adsorbed from the rest gas to a copper surface at the temperature of liquid nitrogen. The yields of secondary ions measured by PDMS are plotted versus the time after cleaning the surface by ion etching. The measurements corresponding to the right column were started 60 s after ion etching and the ones to the left after 20 s.

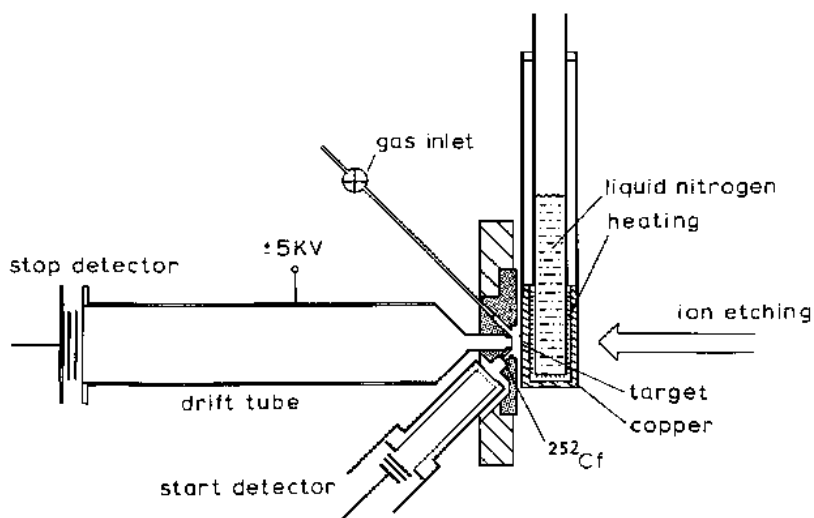


Fig. 2. The TOF instrument used to measure secondary ion mass spectra of frozen gases. The sample carrier, a hollow copper rod, is on ground. The acceleration grid, the drift tube and the stop detector are on a potential of +5 or -5 kV.

dominant ionization process of all heavier molecules. That could explain partially the observed time gap. In the present work the onset of negative ion emission has not been investigated.

3. Experimental method

When the measurements took more than a few minutes at a pressure of 10^{-7} mbar, the mass spectra of the frozen gases were mixed with contaminants (see fig. 1). Therefore, we developed a method to refresh the sample continuously during the measurement of a PD mass spectrum. The corresponding instrument is sketched in fig. 2.

The mass spectra were measured by means of the TOF technique used in most PDMS instruments [48]. The samples were irradiated by the fission fragments of a ^{252}Cf source being located at a distance of 17 mm in front of the sample surface. The vapour of organic material was blown through a teflon capillary (i.d. = 2 mm) onto the copper substrate. The gas flow was regulated by a small needle valve, which was kept on a temperature of about $+100^\circ\text{C}$ in order to avoid condensation of the heavier gases like tetradecane in the valve. The sample substrate, a hollow copper rod, was cooled by means of liquid nitrogen, but could also be heated up to $+400^\circ\text{C}$. The rod was turnable to change the surface seen from the ^{252}Cf source and the exit of the teflon capillary or to clean the surface of the substrate by 4 keV Ar-ion etching. The minimum time between ion etching and the start of a measurement was 20 s. A thermocouple placed 1.5 mm behind the sample deposit in the copper rod was used to control the temperature.

The vacuum chamber of the instrument was divided into two sections: one containing the TOF equipment (the drift tube and the channel plate detectors) and the other containing the copper rod. The only connection between these two chambers was a 7 mm hole being the holder of the acceleration grid. The organic vapour was mainly blown into the second chamber; the pressure established in the first chamber was always less than 10^{-5} mbar. In order to control the speed of sample growth and the cleanness of the sample, the count rate of certain ions was registered in time intervals of typically 10 s. The ions were selected by means of windows set on the lines of interest in the mass spectra. Corresponding growth curves have been shown in fig. 1.

4. The experimental mass spectra

By means of secondary electrons ejected from the sample, the rate of fission fragments impacting the

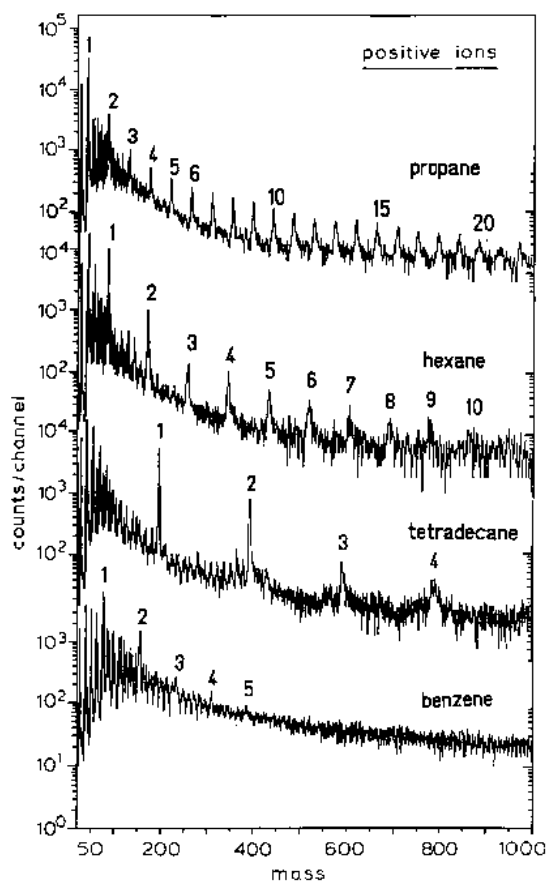


Fig. 3. TOF mass spectra of positive ions ejected by ^{252}Cf fission fragments from frozen alkanes and benzene at a sample temperature of -180°C . Each spectrum was measured for 1 h. On top of the cluster peaks, the number of molecular constituents is given.

effective target area (i.d. = 7 mm) was determined to be $(120 \pm 8) \text{ s}^{-1}$. Absolute ion yields were evaluated with the help of the corresponding electron peak registered in the first channels of each negative ion mass spectrum. The ion detection efficiency of the channelplate detector was estimated to be 60%. The yields of certain ions showed, however, fluctuations within a factor of 2, which were probably caused by the organic vapor let in the vacuum chamber for sample preparation. For pentane, for instance, we determined a total yield of positive ions of 7.9/impact and for negative ions of 4.0/impact. These numbers include all background ions appearing in the mass spectra and also some neutrals generated by metastable decay during flight. Absolute yields of negative ions are presented in fig. 5. Again for pentane, the following absolute yields of positive ions were measured:

$$Y_a((\text{M}-\text{H})^+) = 0.47/\text{impact},$$

$$Y_a(\text{CH}_3^+) = 0.16/\text{impact}.$$

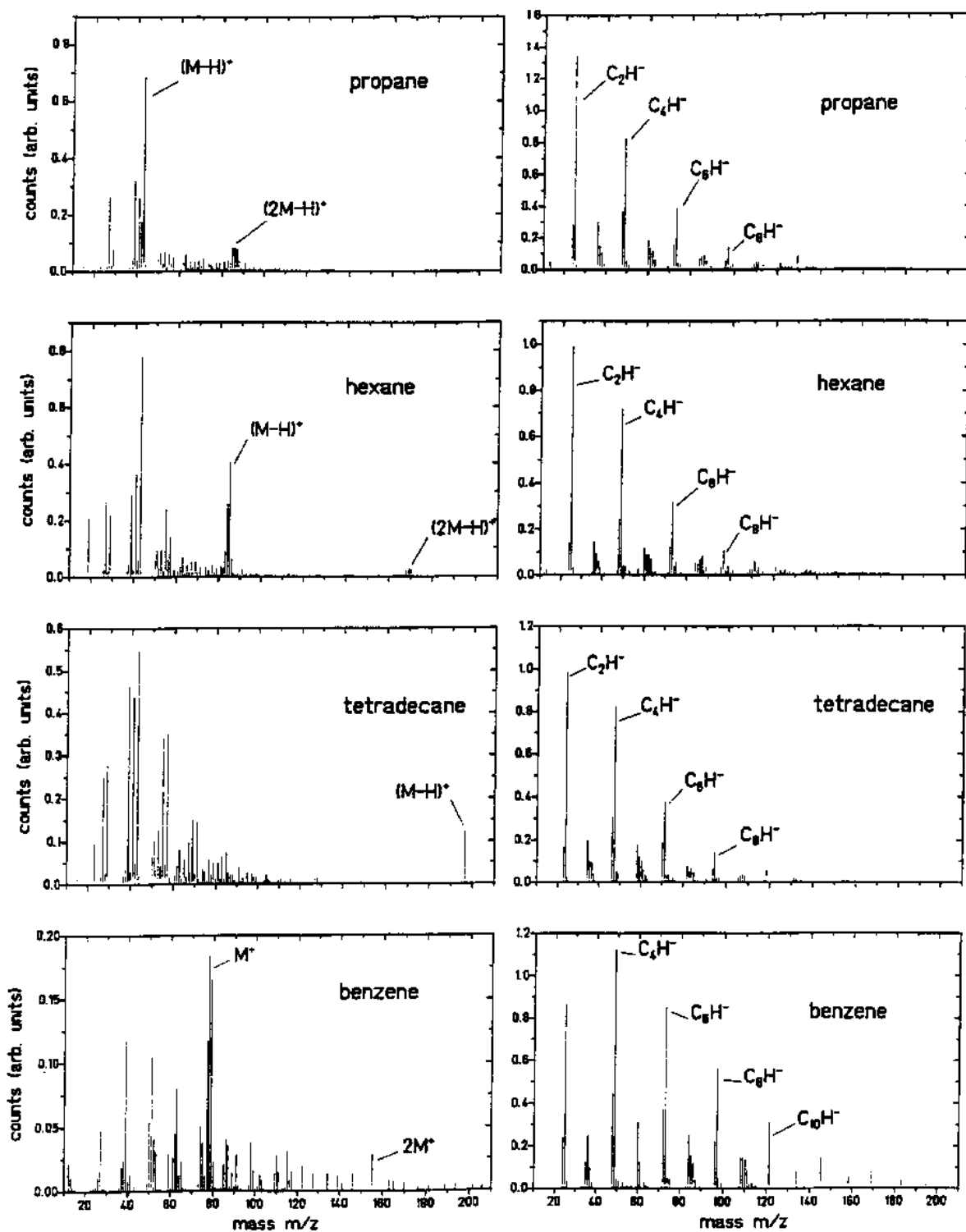


Fig. 4. Mass region between 10 and 210 amu of mass spectra measured with positive (left) and negative (right) ions ejected from alkanes and benzene by ^{252}Cf fission fragments. The ion intensities are given as bars. The background was subtracted. The mass lines are usually not separable above 120 amu. Therefore, a group of several unresolved lines is given by one bar – for instance, the group of the positive parent ions of tetradecane or the group around the $C_{10}H^-$ ion of benzene.

The measurement of one mass spectrum took typically 1 h for the positive ions and 0.5 h for the negative ions. The frozen gas sample was considered to be free of contaminations when the mass lines at $m/z = 16$ (O^+), 17 (OH^-), 19 (H_3O^+), 23 (Na^+), 26 (CN^-) and the lines associated with acetone were missing in the mass spectrum. Nevertheless, contamination could not always be completely avoided as one can see by the small lines at $m/z = 19$, 23 and 59 in the positive spectra shown in fig. 4. In a few negative ion mass spectra a weak line at 35 amu was observed, which we could not attribute to hydrocarbon ions. In case of butane, the absolute yield of this ion was 0.03/impact, in all other cases below 0.005/impact.

As seen in fig. 3 the spectra of positive ions show the cluster series of the molecular ion – pronounced for all alkanes and relatively weak for benzene. The alkane series end usually at about 1000 amu. Corresponding series including the molecular ions have not been found in the negative ion spectra. As already published in ref. [55] the positive molecular ions have the pattern $(M-H_n)^+$ with $n = 0-4$. The most intensive mass line is usually produced by the $(M-H)^+$ ion, whereas protonation is seldom. For benzene the $(M-H)^+$, the M^+ and the $(M+H)^+$ ions have similar intensities.

In fig. 4, bar spectra of the low mass regime are displayed. Each bar corresponds to the count rate of one ion, the background being subtracted. Concerning the negative ion spectra, a striking observation is that the spectra of the 12 different alkanes are hardly distinguishable and that even the benzene spectrum exhibits the same general pattern as the alkane spectra. Negative molecular ions were not observed. As will be discussed further in the next section, the negative spectra are almost independent of the molecular structure – even when the aliphatic alkanes are compared with the aromatic benzene. Contrary to the negative ions, the positive ion spectra presented in the left part of fig. 4 are clearly depending on the molecular structure. That is not only exhibited by the molecular ions and cluster ions but also by the pattern of the hydrocarbon groups having masses below the molecular mass. The number of hydrocarbon groups is generally extended to higher values, when the alkane molecules are longer.

5. Discussion

The fission fragments used in the present experiments deposited an average energy of 640 eV/Å in the frozen samples. About 60% of this energy is primarily stored in the kinetic energy of about 25 electrons/Å [33,31] which generate further secondary

electrons and electronic excitation. In insulators, the atomic system receives energy via low energetic electron scattering, Coulomb repulsion of ions in the positively charged central core [42], and various repulsive recombinations or reactions between molecules or atoms and ions or electrons. Such processes have been reviewed, for instance, by Budzikiewicz [7], Brown and Johnson [6] and Schou [46]. The moving atomic particles initiate low energetic collision cascades [22] and – at high energy densities – also coherent atomic motion leading to erosion-like sputtering at the surface [24,21].

Small-angle scattering of neutrons [2] and X-rays [12] has been used to determine in crystalline material the cylindrical zone of disorder being produced by the passing heavy ion. By means of a semiempirical expression given in ref. [2] we evaluated this radius for tetradecane as

$$r_{am} = 16.3 \text{ \AA}.$$

Recent investigations with an electron transmission microscope have shown that within r_{am} the crystalline material has become completely amorphous. The sharp border between the amorphous and crystalline areas indicate a phase transition – that means, for a certain time interval after the heavy ions passage the material inside r_{am} was liquid or gaseous. By means of the model of nonlinear energy dissipation in the hot central zone propagated by Watson and Tombrello [53], we calculated the mean energy per atom inside r_{am} and obtained

$$\epsilon_{am} = 1.4 \text{ eV/atom}.$$

5.1. Negative ions

If one considers the measured spectra under these aspects, the negative ion mass spectra seem to confirm the molecular destruction in the central zone of the track. Intact molecular ions are not present, only cluster ions are observed being composed either of carbon atoms or of carbon atoms and a few hydrogen atoms. Due to the high degree of destruction, the original structure of the sample molecules seems to be masked by a general mass distribution being not sample specific. Quite similar negative ion spectra have been measured also by gas-phase electron-impact mass spectrometry with alkanes [39,36,34] and benzene [3]. Here, the anion spectra were obtained as a result of monomolecular dissociative electron capture [7] causing an extensive release of hydrogen and fracture of C–C bonds. Such processes can certainly also occur in the surrounding of the nuclear track penetrated by a large number of secondary electrons. The loss of H_2 associated with dissociative electron capture has been in fact observed with frozen methane bombarded by keV ions [20].

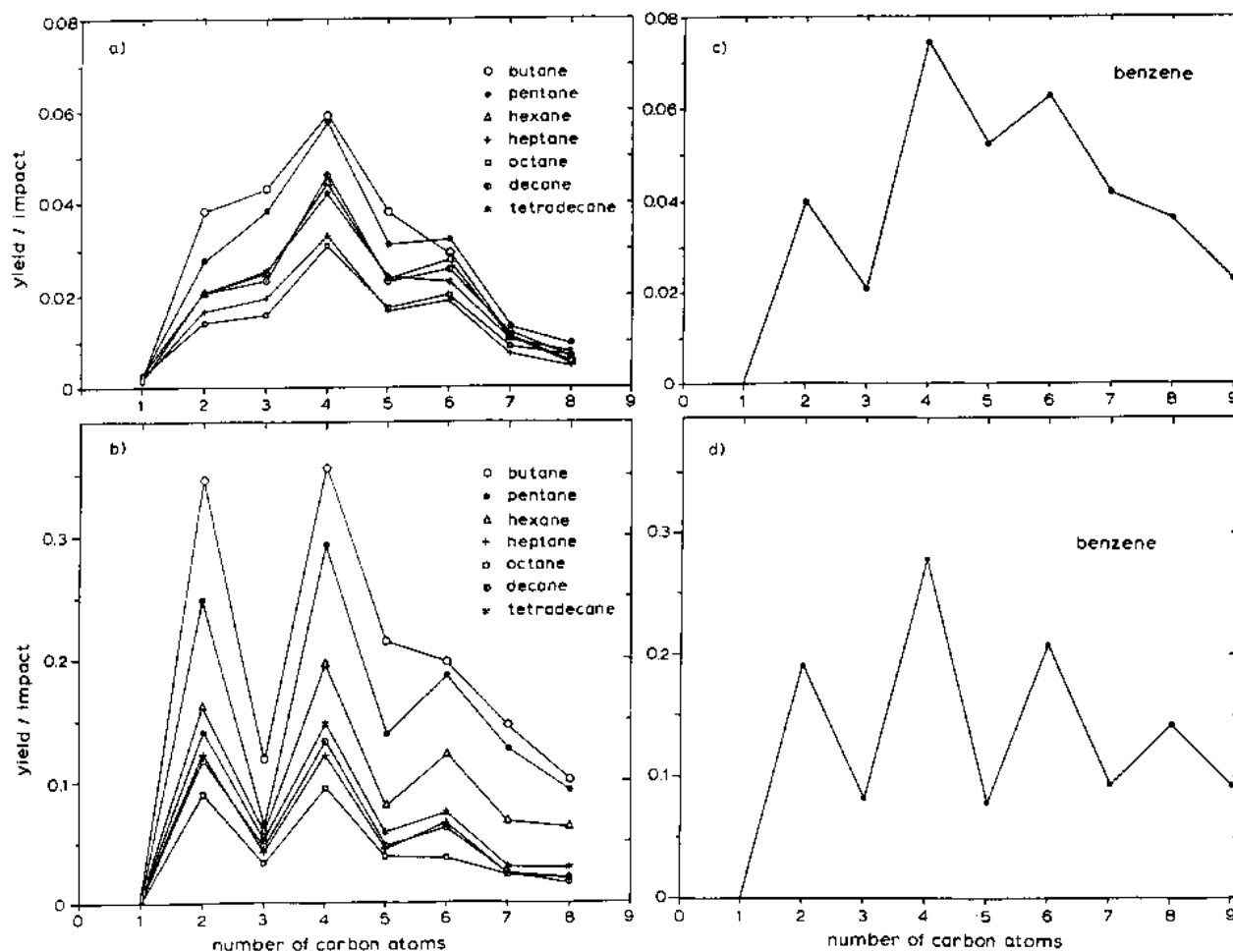


Fig. 5. Absolute yields of carbon cluster ions C_n^- (a and c) and integral hydrocarbon groups $C_nH_m^-$ (b and d) as a function of n , the number of carbon atoms per cluster.

Contrary to the conditions of gas-phase mass spectroscopy, the high density in the energized zone of the track leads to frequent collisional reactions between the dissociation products. As seen in the spectra of fig. 4, the anion yields of the alkanes level down up to mass number 140 – independent of the length of the original molecule. With respect to the mass distributions beyond the molecular mass, a part of the collisional reactions have to be associative. Also in figs. 5 and 6, there is no indication that the mass number or the number of carbon atoms per molecule plays an essential role in negative ion formation. Therefore, it is unlikely that ion–molecule reactions or dissociation of molecular clusters after electron capture are responsible for the final mass distribution alone.

Compared with the enormous number of primary free electrons the total negative ion yield (about 4/impact) is small. Also the total atomic particle yield is two or three orders of magnitude higher [24]. Neg-

ative charging of the observed ions occurs probably during the last collisions in the expanding plume of particles and is governed by the electron affinity of the available products. The carbon clusters C_n have probably the highest electron affinity (2–5 eV [54]) of the possible destruction and reaction products. In figs. 5a and 5c the absolute yields of negatively charged carbon clusters are plotted versus n , the number of atoms per cluster. Characteristic for all alkanes is the maximum yield at $n = 4$ and the odd–even staggering of the yields.

A similar odd–even effect has been reported for negative carbon cluster ions being generated in the vapour above heated graphite [54] or being sputtered from polycarbonate by Cf-fission fragments [18]. The staggering was explained by the fact that the electron affinity is generally higher for even- n clusters than for the neighbouring odd- n clusters. As shown in figs. 5b and 5d, the staggering observed in the present work is

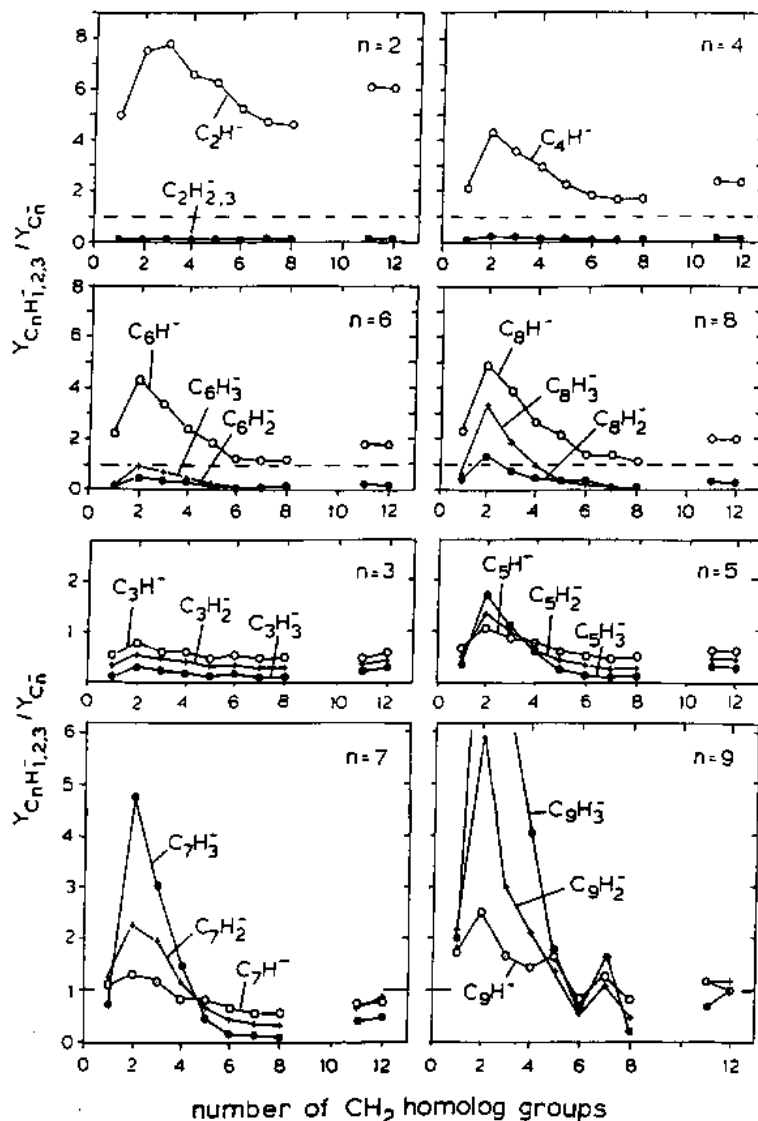


Fig. 6. Relative intensities of $C_n H_m^-$ ions with $m = 1, 2, 3$ plotted versus the number of CH_2 homolog groups of the investigated alkanes. The ion yields are normalized to the yield Y_0 of the pure carbon cluster ions C_n^- . Each figure corresponds to a constant number n of carbon atoms per cluster. Mass spectra of dodecane and tridecane have also been measured. The corresponding data points turned out to lie far above the curves shown in these figures and should be reproduced before presentation.

even more pronounced, when the integral yield of the negative hydrocarbon groups is considered.

As mentioned in section 4, the accuracy of measuring absolute ion yields was limited. Nevertheless, fig. 5b illustrates clearly that the negative ion yields decrease with the molecular weight of the alkanes. An exception is propane having yields close to the values of alkanes being heavier than hexane (see also fig. 6). We are not sure, whether propane exhibits a peculiar desorption phenomenon, or this behaviour is related to its low melting temperature (-189.9°C) being close to the sample temperature (about -195°C).

From several frozen gases it is known that the sputter yield changes when the sample temperature approaches the melting point [46]. The decrease of absolute ion yields with molecular mass is mainly attributed to those carbon-cluster ions having one or more hydrogen adducts. This is demonstrated in fig. 6. Here, we present for ten alkanes the relative $C_n H_m^-$ yields ($m = 1, 2, 3$) normalized to the yield of C_n^- . From butane (number of CH_2 -homolog groups = 2) to octane (= 6), the $C_n H_m^-$ yields decrease within a hydrocarbon group and remain then almost constant up to tetradecane. The effect is most pronounced for

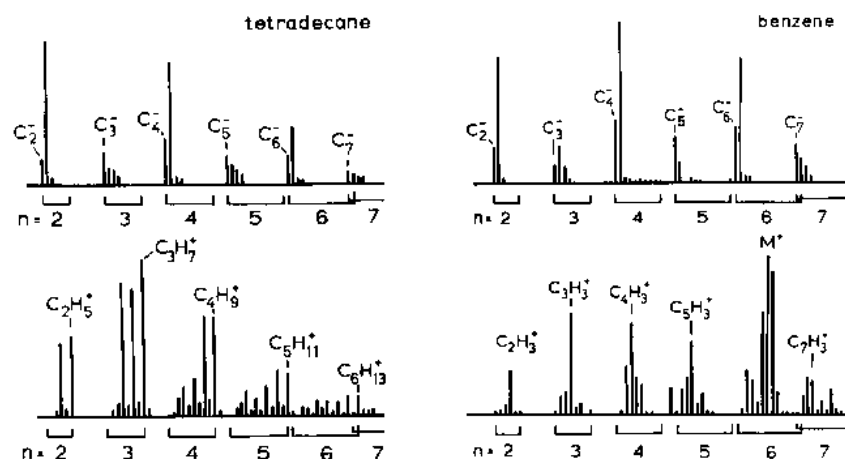


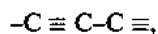
Fig. 7. General structure of the hydrocarbon PD mass spectra measured with tetradecane and benzene between 20 and 95 amu. The dashed line shown in the middle of the positive benzene spectrum indicates a small acetone contamination ($M+H=59$ amu).

the $n = 9$ groups, where the C_n^- yields are equal within $\pm 50\%$. So far, we do not have a plausible explanation of this phenomenon. The hydrogen-carbon ratio in the central zone of the nuclear track is eventually important. Butane contains only 10% more hydrogen than octane, but heavier alkane molecules might lose a larger fraction of their hydrogen after dissociative electron capture than the lighter ones.

We suppose here that the number of hydrogen adducts is related to the number of free carbon bonds. In the negative spectra, the strongest mass lines are produced by the even- n ions C_nH^- , whereas the associated $C_nH_2^-$ and the $C_nH_3^-$ ions are either weak or missing (see also fig. 6). The basic carbon clusters of this even- n series should have two free bonds – one always occupied by the negative charge. That leads to an acetylenic-type of bonding:



Carbon clusters with two free bonds can also be formed by cyclic structures, but these have only recently been observed [14] below $n = 10$ in comparison to ref. [54], and seem to need comparatively longer production times. The carbon clusters of the odd- n groups seem to have four free bonds, because up to three hydrogen adducts are observed. The corresponding bonding type – for instance for $n = 3$ – could be again acetylenic,



or cumulene,



or cyclic.

5.2. Positive ions

As shown in figs. 3 and 4, the positive mass spectra exhibit molecular ions and molecular cluster ions. But also the substructure of the hydrocarbon groups is characteristic for the sample compound as illustrated in fig. 7, where the low mass regions of positive and negative spectra are compared. The numbered brackets under the well separated hydrocarbon groups mark the mass range between the pure carbon clusters C_n and the aliphatic fragment C_nH_{2n+1} , which corresponds to the cleavage of a C-C bond of an alkane molecule. In fact, for the alkanes, the most intense ion of each group is the C_nH_{2n+1} fragment. This behaviour is similar to spectra measured by means of gas-phase electron-impact mass spectroscopy. In the present spectra, dehydration – i.e. abstraction of H_2 – is well expressed by strong mass lines 2, 4, 6, ... mass units below the $C_nH_{2n+1}^+$ ion – probably because the mean internal energy of the fragments is higher than after a 70 eV electron impact.

In the positive benzene spectrum, the aromatic bonding type of the molecule seems to be important for the substructure of the hydrocarbon lines. Purely aliphatic ions are rare, the strongest mass lines are generated by the $C_nH_3^+$ ions having only double bonds between the carbon atoms. Accordingly the number of hydrogen adducts is smaller than in most alkane fragments.

The investigation of angular distributions has shown that large molecular ions are not ejected from the infratrack (see ref. [17]), but that has not been verified for smaller molecules [40]. When the positive alkane-fragment ions are generated via collisional reactions in the inner track zone, one should observe

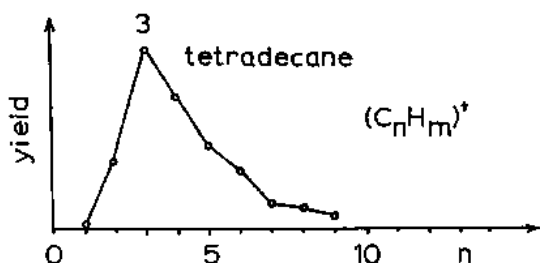


Fig. 8. Integral yields (arbitrary units) of groups of positive hydrocarbon ions plotted versus the number of carbon constituents. The data have been measured with tetradecane.

positively charged carbon cluster ions as in the negative mass spectra. Corresponding C_n^+ signals are either very weak or not present. On the other hand, C_n^+ ions are known to exist above heated graphite [54] and they are also reported in PDMS work. Feld et al. [18] found such cluster ions in PDMS spectra of polycarbonate, polyvinylidene fluoride and other polymers. Also the odd-even staggering of the integral $C_n H_m^+$ yield observed by Feld et al. does not exist in the present spectra, as demonstrated in fig. 8.

It seems to be plausible that positively charged hydrocarbon species are formed in the positively charged infratrack. There exists, in fact, experimental evidence that the infratrack is positively charged for a short time interval after the heavy ions passage [44]. The attributed track potential decays rapidly, because only the relatively fast hydrogen ions experience its electrical force [37,40,19]. The formation and ejection of heavier – and slower – ions has not found to be influenced by any track potential – i.e. charging of the infratrack.

5.3. Conclusions concerning the experimental data

Regarding the pattern of corresponding negative and positive hydrocarbon groups, the degree of hydrogen abstraction is obviously related to the amount of internal excess energy – being high after electron capture and lower after ionization by electron impact. The general mass distribution of negative ions implies frequent and partially associative collisions between nonspecific destruction products, which are probably generated inside a plasma along the nuclear track. The positive ions could be explained simply by dissociation of molecular ions and molecular cluster ions – comparable to ion formation in the gas phase by electron impact. Our conclusion is that positive fragment ions are not residues of the vigorous destruction process inside the inner track zone. They seem to be decay products of excited molecular ions, which are eventually ejected from the first monolayer at the surface and which experience only a small number of collisions.

This conclusion seems to be contrary to experimental findings with Langmuir–Blodgett films [43,45], but the peculiar ordering of such films might lead to a desorption behaviour different from that of frozen alkanes or benzene. Ion production by molecular or cluster decay into ion pairs is probably of minor importance, because recent studies of ion-pair correlations [47] gave only small correlation coefficients (< 10%).

6. Model calculations

6.1. Introduction

For ions being desorbed in PDMS and assumed to come from the ultratrack, longstanding theoretical calculations have unraveled basic parts of the complicated desorption mechanism such as the electronic energy deposition [33], the transport and recombination to mechanical energy [31,15,16,26], the mechanical shock wave release of energy [30,25] and finally the desorption of molecules [32] and their subsequent ionization. Specifically, the desorption of positive hydrocarbon ions from regions away from the hot central core has been studied recently [28]. There the gross features of the experimental distribution of hydrocarbon fragments were studied by breaking the carbon backbone of the hydrocarbon chain. We used two model assumptions, a thermal breakup as known from EI, and an entropic breakup where each carbon-carbon bond picks up energy from the passing-by secondary electron pulse independent of each other in a very short time (compared to bond vibrations). The entropic process assumption could readily explain the general pattern of the homologue fragment ions abundances with the maximum at $n = 3$ in contrast to the thermal breakup where it comes out to be $n = 4$, as e.g. known from positive ion EI-spectra of hydrocarbons.

Here we complement this by investigating the hydrogen release and the clusterization of the desorbed material.

Before this, we dwell further on the fate of the material from the innermost part of the primary ion track. It has been proposed that in this track a perhaps totally atomized plasma is formed which then should expand adiabatically into the vacuum. While the gas cools down, the aggregation to new small molecules and clusters is assumed [28]. Even the formation of fullerenes has been advertized for the special case of a PVDF foil as sample material [49,5]. Earlier studies which explicitly mention this mechanism as a possible pathway to desorbed light ions are given by Feld et al. [18], also for the case of carbon material. In the following section we will show new aspects of this model including the setup of reaction network calculations.

The final distribution of molecular ions depends on the history of temperature, density and composition of the ejected material. It should be noted, however, that due to later processes the earliest part of the history is hard to be read off from the final experimental spectra. So, different models, with different process paths in the beginning but a similar history later may give similar results. The initial temperature and density is set by the physics of the process.

6.2. Cluster formation from the infratrack

6.2.1. Adiabatic expansion model

As described in section 5 the material of the infratrack is assumed to be fully atomized in the beginning of the process and subsequently ejected into the surrounding vacuum expanding adiabatically. We take the radius of the infratrack as a parameter between 5 and 20 Å because the exact value is not known yet. For carbon or hydrocarbon material we have calculated the time-dependence of the temperature as well as the mean free path of the particles and the adiabatic expansion velocity of the gas, which we give as a function of distance from the sample surface (see figs. 9, 10 and 11). For a detailed description of these calculations see ref. [8]. The radius of the inner track and the electronically deposited energy dE/dx are the decisive parameters.

6.2.2. Formation of new clusters and molecules

We study the formation of new molecules and clusters by collisions in the expanding gas. Important factors for the formation are the collision rate, which depends on the velocity of the particles and the density of the gas, and the internal excitation energy of the colliding partners, which varies with temperature. These parameters are obtained from the adiabatic expansion model.

Experiments [14,52,1] have shown that even for small carbon and hydrocarbon clusters various isomeric structures do exist, such as a rhombic and a linear structure for C_4 . There should be different formation probabilities for these isomeric structures. This is described by a steric factor P which is dependent on the rotational and vibrational partition functions of the reactants and the products [35]. Including these factors we get for the rate of formation R [35]:

$$R = PZ_{AB}^0 \exp(-E_0/kT) c_A c_B,$$

where c_A , c_B are the concentrations of the reactants, E_0 is the activation energy of the complex and Z_{AB}^0 is the collision rate,

$$Z_{AB}^0 = \pi d_{AB}^2 (8kT/\pi\mu)^{1/2}.$$

μ is the reduced mass of A and B and d_{AB} is their interaction radius. The aggregation of bigger clusters,

the loss of single atoms and the decay of clusters has been described by a network of differential equations, which then is solved numerically. With these ingredients we are at present calculating a large network of reactions between carbon and hydrogen atoms and clusters. Qualitative features will be discussed here in close connection to experimental data.

6.2.3. Comparison with experimental data

Comparison of the results with the experimental data shown in sections 4 and 5 should give information about the structure of the newly formed particles. When looking at the negative spectra, we observe a distribution which is typical for all hydrocarbon materials and does not depend on the structure or the molecular mass of the sample. Pure carbon clusters can be interpreted as nonlinear structures, whereas the C_nH^- molecules may be acetylenic chains, see section 5. Vager et al. [52] experimentally obtained nonlinear structures for C_n clusters, $n = 4, 5, 6$, with the Coulomb explosion imaging technique. The electron affinities that they measured are lower than those found for linear chains. The well known odd-even alternation in electron affinity for clusters with $n > 10$, where electron affinity is lower for even numbers of carbon atoms, is now found for nonlinear structures down to $n = 4$.

The different behaviour between linear and nonlinear structures concerning the attachment of hydrogen atoms as proposed in ref. [14] could be another hint: Doverstål et al. [14] studied the reaction of small carbon clusters with hydrogen during laser vaporization. They found differences in the aggregation of hydrogen when varying the experimental conditions. The attachment of hydrogen is increased by increasing the vaporization laser power. They propose that the dissociation of molecular hydrogen is improved and carbon clusters are excited. When cooled down, hydrogen recombines and the rate of reaction decreases. They also found different saturation limits for chains and rings. In their spectra the C_nH_2 peaks are very strong. These peaks may belong to the chains where the ends are the most reactive sites and if the collision frequency is high, enough hydrogen atoms will attach. However, if the time between collisions with hydrogen atoms is long enough, carbon chains may form rings. Initially formed rings can react with more than two hydrogen atoms. The respective mass lines of all these forms measured and discussed by Doverstål et al. are present in the negative PDMS spectra of pure hydrocarbons. Thus this may be a hint that different distances to the primary ion track contribute differently having passed different temperature and density histories. Doverstål reports that the characteristic H-reactions are only important if no other carrier gas

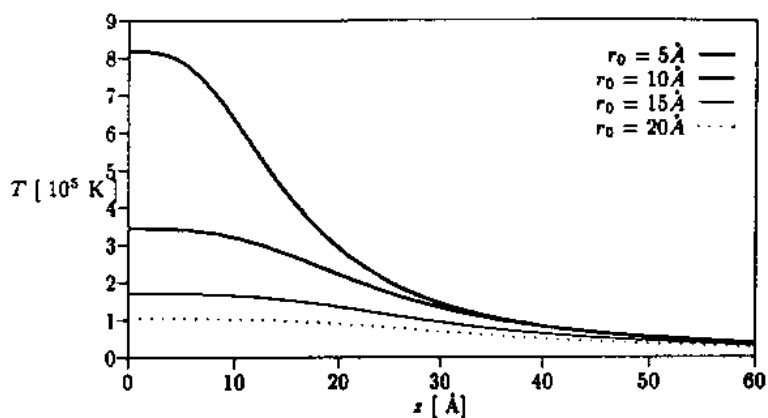


Fig. 9. Evolution of temperature as a function of distance z from the sample surface. $T(z) = T_A (V_A/V(z))^{\kappa-1}$, with T_A the initial temperature, V_A the volume of the inner track, $V(z)$ the volume of the expanding gas (simplified as a cone), and κ the adiabatic exponent.

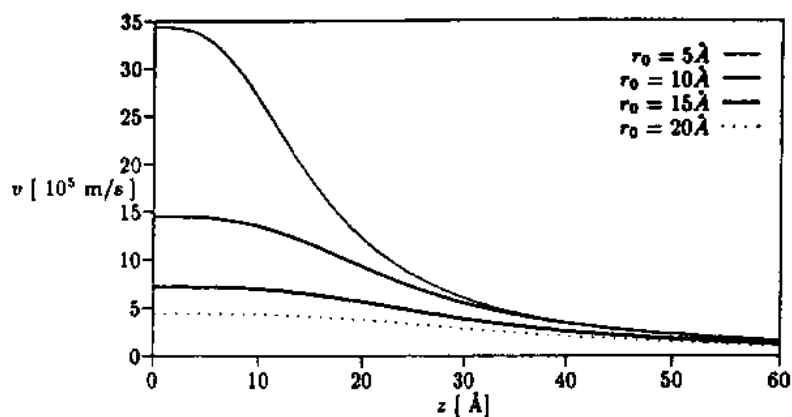


Fig. 10. Evolution of adiabatic expansion speed. $V_{ad} = (2\kappa/(\kappa-1))^{1/2} (k_b/m)^{1/2} T_0^{-1/2} T(z)$, with k_b the Boltzmann constant, and T_0 taken to be 300 K.

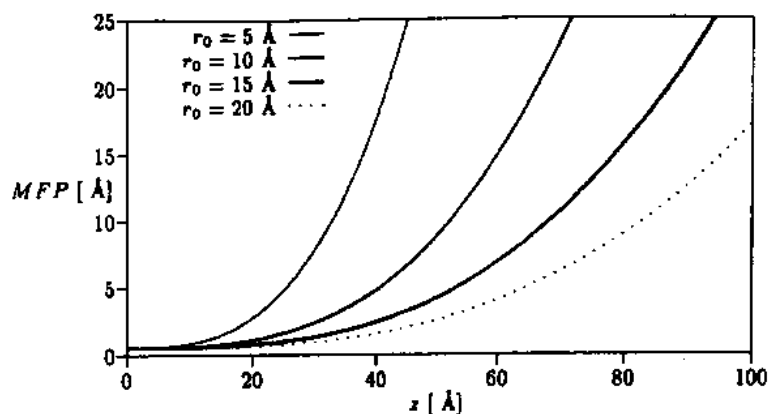


Fig. 11. Growth of mean free path as a function of distance z from sample surface. $MFP = V(z)/(4\pi\sqrt{2}r_{atom}^2 N(V_A))$, with $N(V_A)$ the initial number of particles.

is present, which coincides with our observation that compounds containing nitrogen, oxygen etc. do not exhibit the typical patterns that we find for all pure hydrocarbon compounds.

7. Ions from the ultratrack

The ions from the ultratrack, clusters, molecules or molecular fragments, are studied now. We will use the phrasings *entropic* and *thermal* here to distinguish between processes of different time scale and excitation energies involved.

A *thermal* process is assumed if the time scale of the process is long as compared to chemical bond vibration periods, so that eventual molecular excitation energy will be statistically distributed over the entire molecule. Thermal breakup is encountered if in the breakup process all exit channels contribute, even those which rearrange the structure of the molecule (e.g. McLafferty transitions are rarely found in PDMS spectra, although common in EI spectra). This normally is the case if the molecular excitation energy is small so that only the lowest collective degrees of freedom leading to breakup can be reached. The collision-induced ionization is a typical thermal process. Also, the kinetic energy distribution and the internal molecular vibration spectrum show the same temperature in their distribution.

A process is called *entropic* when its time scale is smaller than the vibrational periods of the molecule. The initial molecular excitation by secondary electrons in the PDMS process is known to be entropic [31,15]. Each chemical bond gets its own breakup chance independent of another. Entropic processes normally involve molecular excitation energies far above a single ionization energy. As known from quantum-mechanical time-dependent perturbation theory in this case the breakup chance is proportional to the inverse of the perturbation time. In PDMS the passing-by secondary electrons set the scale: the inverse of the Rydberg time $\delta t/\hbar$ plays the same role as the temperature in a thermal process. With $(\delta t/\hbar)^{-1} = 10^4$ K in units of the thermal energy scale Kelvin it was readily understood [15] that the kinetic velocity distribution of the desorbed ions has a Boltzmann-like kinetic energy distribution of exactly that energy, and still the ions are internally often entirely cold.

7.1. Comparison to EI spectra

The mass spectral groups due to "breaking the carbon backbone" of the alkanes have been studied in detail for PDMS in ref. [28]. The conclusion there was that this feature of the PDMS spectra is understood

best if the basic mechanism of breaking the carbon bonds is *entropic*. There, the C-C bond breakup probability for the PDMS resulted to be about 0.1. The low end part was somewhat mimicked, the ionization probability being influenced through the late part of the desorption. Thus the largest carbon group peak for all alkanes is at $n = 3$. The EI spectra of the respective alkanes look pretty similar, however they always show the largest peak at $n = 4$, and for larger alkanes at $n = 7$ as well. These peaks can be understood [28] by a *thermal* breakup of the carbon chain.

We supplement this comparison here by studying the carbon group satellite lines due to the loss of hydrogen atoms.

Finally we will present an *entropic breakup* model for the molecular cluster series in PDMS which is not observed in the EI-spectra of the alkanes.

8. Hydrogen detachment of ions from the ultratrack

8.1. Entropic detachment

We assume that the process to desorb and ionize the positive ions of pure hydrocarbons is sequential: First, the carbon backbone is entropically broken during the desorption process. Then, the fragments are released carrying some intramolecular energy as internal excitation. An important channel for this is the subsequent detachment of hydrogen. The overlapping wave functions of neighbouring hydrogens in the CH₂ chain lead to a favoured detachment channel – i.e. the separation of H₂ molecules. We study this by two alternative model assumptions, entropic and thermal H₂ detachment, and for simplicity neglect here the more rare single hydrogen detachment.

Modelling an entropic detachment of H₂ we calculate for a given hydrocarbon the positive ions $(C_n H_{2n+1-2\nu})^+$ as a result of breaking the C backbone of the molecule, the abundance of ions with the same n but sequential loss of H₂. We assume here that the detachment of any H₂ is independent of any other.

For a hydrocarbon fragment of n carbon atoms we have $b = (n - 1)$ C-C bonds. We assumed an independent detachment probability of each of ν H₂. The yield $Y(\nu)$ of fragment ions with the same number n of carbon atoms but a loss of ν H₂ then becomes

$$Y(\nu) = \binom{2b}{\nu} w_0^\nu. \quad (1)$$

This is already normalized to the yield of the fragment with the same number of carbon atoms but no H₂ loss, thus with $\nu = 0$. An easy way to obtain a value for w_0 from an experiment is to calculate the ratio of neighbored ion intensities,

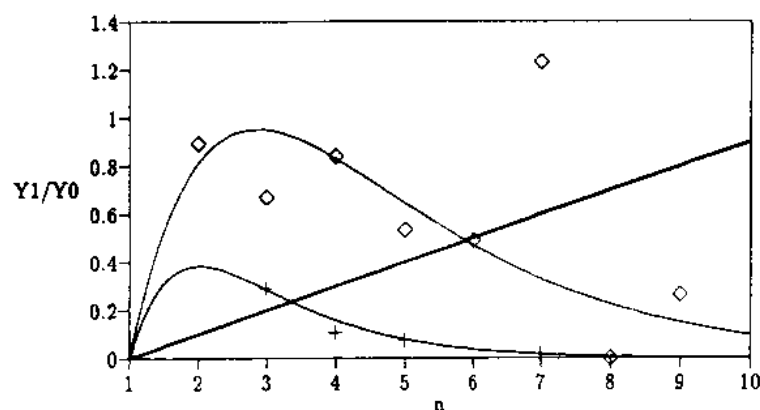


Fig. 12. Hydrogen loss from positive hydrocarbon fragment ions. PDMS (rhombic points) and EI (crosses) experimental yield ratios Y_1/Y_0 for nonane fragment ions of one to no loss of H_2 are plotted. The theoretical curves are obtained by eq. (2) for the assumption of an entropic detachment (linearly rising curve), and by eq. (3) for an assumed thermal detachment, with $b_{PDMS} = 0.18$ and $b_{EI} = 0.33$ (lower curve).

$$\frac{Y_{\nu+1}}{Y_{\nu}} = \frac{2b - \nu}{\nu + 1} w_0. \quad (2)$$

We adopt the value $w_0 = 0.2$ as an empirical value to be compared to the result of quantum-mechanical time-dependent breakup calculations with final state interaction. It is supportive that even different fragments of tetradecane give fairly similar values of w_0 , although the data are scarce and not very accurate for this purpose. However, the ratio $Y_{\nu=1}/Y_{\nu=0}$ rises linearly with b , see fig. 12, in apparent contrast to experiment. We thus conclude that the hydrogen release is *not* entropic.

8.2. Thermal detachment

As an alternative we set up a model for a thermal detachment of H_2 , again neglecting the more rare single hydrogen detachment from the end-groups of the linear alkane molecular structures, including the ionization. For an alkane fragment with n carbon atoms we distribute the excitation energy E , picked up in the process of fragmentation onto the $3n + 1$ covalent bonds. Then we obtain for the thermal detachment of H_2 with $b := \epsilon/E$, the ratio of the H_2 detachment energy to the total excitation energy,

$$Y_1/Y_0 = (2n - 2) \exp(-b(3n - 1)), \quad (3)$$

and

$$Y_2/Y_1 = (2n^2 - 7n + 7)/(n - 1) \times \exp(-(b(3n - 4)/(1 - b))), \quad (4)$$

for the ratios of the yields Y_{ν} of ν H_2 detachments, with $\nu = 0, 1, 2$. The result of this simple model is given in fig. 12. We fitted the only parameter b to the experimental data of the alkane *nonane*, both for PDMS and for comparison to EI. In contrast to the

entropic model given before we get a fair agreement. The values for b are $b_{PDMS} = 0.18$, and $b_{EI} = 0.33$, respectively; the molecular excitation energy in EI is twice as high as in PDMS. We conclude that dehydrogenation of pure hydrocarbons is thermal and therefore takes place well *after* the initial entropic part of the total desorption PDMS. Indeed, Pedrys et al. [41] found that neutral H_2 from the surface emerges thermally, not only from the desorbed material but also by diffusion from the left-over material.

8.3. Entropic breakup of desorbed matter into clusters

The positive ion spectra presented in fig. 3 show cluster series up to about 1000 amu. It is interesting that the maximum number of carbon atoms per cluster (propane, hexane and tetradecane) is about the same in all cases, $n_{max} \leq 80$, but different for the aromatic benzene being another class of substance.

Desorption from the ultratrack region is simulated here by entropic degradation and subsequent breakup. The probability to find a piece of matter, a cluster, is set proportional to the product of all independent breakup probabilities of all bonds from the surface of a cluster to atoms of the neighbouring clusters. We assume that these bonds are bound by van der Waals-type forces. The resulting formula for the yield of a cluster of volume V_c , mass m in amu, and k molecules with n carbon atoms, has then a peculiar algebraic structure,

$$Y(m_c) = \frac{1}{\sqrt{m_c}} \frac{V}{V_c} w_0^{cF_c/F_m}, \quad (5)$$

where F_c is the cluster surface area and F_m the aspect of one molecule. We added the factor $1/\sqrt{m}$ for reasons described below. Here, w_0 is the van der Waals

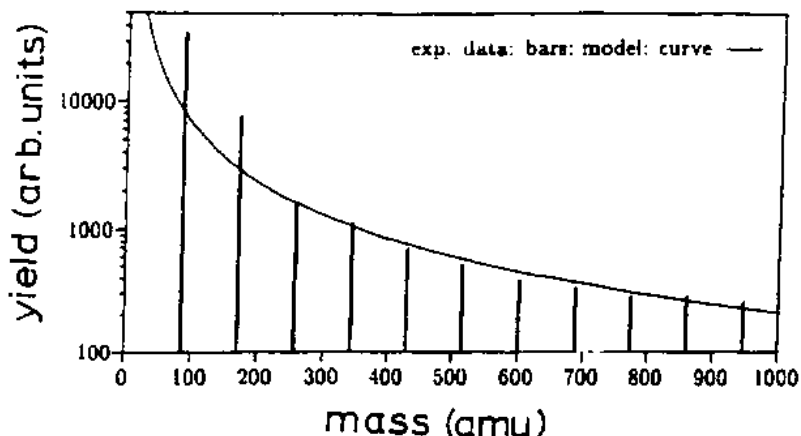


Fig. 13. Yield of positive cluster ions ejected from hexane. The experimental cluster yields, given as bars, are sums over all hydrogen-satellite lines in the spectra. The individual mass yields have been extracted from the experimental time-bin spectrum (see fig. 3) by the software package PEAKS [11] with a low resolution of 2×10^{-2} . The theoretical curve was calculated by means of eq. (5).

breakup probability, V the total desorbed crater volume and V_c the volume of one cluster of mass m_c . We use for the alkanes $V_c = knv_1$ with a matter density of roughly 1 g/cm^3 and thus $v_1 = 23 \text{ \AA}^3$ for CH_2 .

With the values $V/V_c = 8.3 \times 10^6/m$, $w_0 = 0.8$ and $c = 0.195$ in eq. (5) we obtained the curve in fig. 13. Compared with experiment the agreement is surprisingly good over one order of magnitude.

In this model V is just the volume of the crater material which undergoes the entropic explosion – the area of entropic cluster desorption, where the mean energy per molecule is well above the amorphization energy. For the values adopted here we obtain for an assumed hemisphere of the left-over crater a radius of 41.4 \AA . That is consistent with the radii deduced from other experimental data discussed in section 5.

The main discrepancy between model predictions and experiment is that we have to assume the factor $1/\sqrt{m}$ to get a good fit, which does not stem from the model. This additional factor, normalized to $m = 1$, is attributed to a general experimental sensitivity function of PDMS-TOF machines being less sensitive for larger masses. $1/\sqrt{m}$ would thus be a rough analytical guess, which has to be checked with the same type of TOF machine.

The logarithm of the yield Y studied here and compared to experiment is rather insensitive to adjustments of the parameter c . In accordance to the results of fig. 13, we used $c = 0.195$ in contrast to $c_{\text{altern.}} = 1$, if one would divide the surface of a cluster by the aspect of the volume a molecule occupies. However, this "dense" packing is a rather unrealistic description of the space occupation of an alkane and the bonding to its neighbours. A more realistic model should give a smaller value. An alternative formulation would be that the van der Waals cross section is larger than

the geometric aspect used in the context of the dense packing assumption.

The experimental time of flight spectra are given with constant *bin* size. The ion time of flight distributions for one ion mass, however, become wider according to $\delta k = \frac{1}{2}a(\delta m/m)\sqrt{m}$. With the resolution $\delta m/m$ being experimentally constant, δk grows as \sqrt{m} . Thus a given number of ions of the same mass spreads over a number of time bins proportional to $1/\sqrt{m}$.

In addition one has to sum over all mass lines of the same number of carbon atoms but different H_2 -detachments (see refs. [13,28]). Thus in the case of *hexane*, the experimental data are extracted here and replotted. We used the code PEAKS [23,27,10,9]) for extracting the number of ions of one mass, and then added these integrals. For the results, see fig. 13.

We tried different model assumptions, such as a breakup proportional to the volume or the area of the surface of the clusters but these gave different functional behaviours and could not fit the experiments. Thus the comparison to the experiments in fig. 11 seems to favour the mechanism of an independent breakup chance for all intramolecular bonds in the desorbed material, as typical for entropic electronic excitations in PDMS.

9. Conclusions concerning the model calculations

The formation of negative carbon cluster ions has been modeled using the extreme assumption of an adiabatically expanding atomized gas ejected from the interior part of the primary ion track. The formation of molecular clusters, as found in the positive ion fragment spectra has been modeled with an entropic ("ex-

plosive") model. Finally the hydrogen satellite lines of the positive ion spectra of the studied alkanes are compared to results of models for different mechanisms, especially the thermal H₂-detachment of the formed molecules, clusters and fragments after desorption.

Acknowledgements

We acknowledge the close collaboration with J. Curdes and B. Dickmann.

References

- [1] Y. Achiba, C. Kittaka, T. Moriwaki and H. Shiromaru, *Z. Phys.* D19 (1991) 427.
- [2] D. Albrecht, P. Armbruster, R. Spohr, M. Roth, K. Schaupert and H. Stuhmann, *Appl. Phys.* A37 (1985) 37.
- [3] R. Aplin, H. Budzikiewicz and C. Djerassi, *J. Am. Chem. Soc.* 87 (1965) 3180.
- [4] I.S. Bitensky and E.S. Parilis, *Nucl. Instr. and Meth.* B21 (1987) 26.
- [5] G. Brinkmalm et al., *Chem. Phys. Lett.* 191 (1992) 345.
- [6] W. Brown and R. Johnson, *Nucl. Instr. and Meth.* B13 (1986) 295.
- [7] H. Budzikiewicz, *Angew. Chemie* 93 (1981) 635.
- [8] B. Curdes, Cluster-bildung schwerionen-induzierter desorption, M.S. Thesis, University of Oldenburg (1993).
- [9] J. Curdes, P. Borrmann, E.R. Hilf and W. Tuszynski, *Proc. ASMS92 (Am. Soc. Mass Spectr., 1992)* p. 567.
- [10] J. Curdes and E.R. Hilf, *Fresenius Z. Anal. Chem.* 344 (1992) 140.
- [11] J. Curdes and E.R. Hilf, PDMS analysis tools, in preparation (1993).
- [12] E. Dartyge, J.P. Durand, Y. Langvin and M. Maurette, *Phys. Rev.* B23 (1981) 5213.
- [13] B. Dohmen et al., *Proc. ASMS92 (Am. Soc. Mass Spectr., 1992)* p. 570.
- [14] M. Doverstål, B. Lindgren, U. Sassenberg and H. Yu, *Z. Phys.* D19 (1991) 447.
- [15] B. Nitzschmann, E.R. Hilf and H.F. Kammer, Mechanism of desorption, in: *The Analysis of Peptides and Proteins by Mass Spectrometry*, ed. C. McNeal (Wiley, 1988).
- [16] B. Nitzschmann, E.R. Hilf and H.F. Kammer, Computer simulations of FHIID, in: *Mass Spectrometry of Involatile Material Ion Formation from Organic Solids (IFOS IV, 1987)*, ed. A. Benninghoven (Wiley, 1989).
- [17] W. Ens, B.U.R. Sundqvist, D. Hakansson, A. Hedin and G. Johnson, *Phys. Rev.* 1339 (1989) 763.
- [18] H. Feld, R. Zurmühlen, A. Leute and A. Benninghoven, *J. Phys. Chem.* 94 (1990) 4595.
- [19] D. Fenyö, A. Hedin, P. Hakansson and B. Sundqvist, *Int. J. Mass Spectrom. Ion Process.* 100 (1990) 63.
- [20] G. Foti, L. Calcagno, F. Zhou and G. Strazzulla, *Nucl. Instr. and Meth.* B24/25 (1987) 522.
- [21] W. Guthier, *Proc. Third Int. Workshop on Ion Formation from Organic Solids, IFOS III, Münster, 1985*, ed. A. Benninghoven, *Springer Proc. Phys.* 9 (1986) 17.
- [22] P. Haff, *Appl. Phys. Lett.* 29 (1976) 473.
- [23] S. Harsdorf, E.R. Hilf, B. Nitzschmann, W. Schlez, J. Thomaschewski, K. Koch and P. Wagner, in: *Mass Spectrometry of Large, Non-Volatile Molecules for Marine Organic Chemistry*, vol. 3 of *Int. Workshops on the Physics of Small Systems*, eds. E.R. Hilf and W. Tuszynski (World Scientific, 1990) p. 164.
- [24] A. Hedin, P. Hakansson, M. Salehpour and B. Sundqvist, *Phys. Rev.* B35 (1987) 7377.
- [25] E.R. Hilf, *Int. J. Mass Spectrom. Ion Process.* 125 (1993) to be published.
- [26] E.R. Hilf, H.F. Kammer and B. Nitzschmann, *Proc. Int. Symp. on swift heavy ions in matter, SHIM*, eds. J. Remillieux, P. Armbruster and J.C. Jousset (1989) p. 93.
- [27] E.R. Hilf, W. Schlez, K. Kruse, A. Dullweber, U. Steenen, S. Harsdorf, K. Koch, B. Nitzschmann, H.F. Kammer and W. Tuszynski, in: *Software Development in Chemistry V*, ed. J. Gmehling (Springer, Berlin, Heidelberg, 1991).
- [28] E.R. Hilf, W. Tuszynski, B. Curdes, J. Curdes, M. Wagner and K. Wien, *Proc. Int. Workshop on PDMS, Gaspe, Canada, 1992*, *Int. J. Mass Spectrom. Ion Process.* 125 (1993) to be published.
- [29] R.E. Johnson, B.U.R. Sundqvist, A. Hedin and D. Fenyö, *Phys. Rev.* B40 (1989) 49.
- [30] H.F. Kammer, in: *PDMS and Clusters*, vol. 269 of *Lecture Notes in Physics*, eds. E.R. Hilf, H.F. Kammer and K. Wien (Springer, Berlin, Heidelberg, 1987) p. 107.
- [31] H.F. Kammer, Elementary Electronic Processes in Electronic Sputtering, Ph.D. Thesis, University of Oldenburg (1991) and references therein.
- [32] H.F. Kammer and E.R. Hilf, in: *MeV and keV Ion and Cluster Interactions with Surfaces and Materials*, vol. 2 of *Proc. 2nd Int. Workshop, Orsay, 1988*, eds. Y. LeBeyec et al., *Wangerooze Series of Int. Workshops on PDMS* (1989) p. 245.
- [33] H.F. Kammer and E.R. Hilf, *Proc. Ion Formation from Organic Solids (IFOS V)*, 1989, eds. A. Hedin, B.U.R. Sundqvist and A. Benninghoven (Wiley, 1990) p. 197.
- [34] V. Khvostenko and G. Tolstikov, *Russian Chem. Rev.* 45/2 (1976) 127.
- [35] J.H. Knox, *Molecular Thermodynamics* (Wiley, 1978) chapter 12.
- [36] L.V. Trepka and H. Neuert, *Z. Naturforsch.* 18a (1963) 1295.
- [37] R. Macfarlane and D. Jacobs, *Proc. Fourth Int. Conf. on Ion Formation from Organic Solids, IFOS IV, Münster, Germany, 1987*, ed. A. Benninghoven (Wiley, 1989) p. 71.
- [38] R.D. Macfarlane and D.F. Torgerson, *Science* 191 (1976) 920.
- [39] C. Melton and P. Rudolph, *Chem. Phys.* 31/6 (1959) 1485.

- [40] R. Moshhammer, Ph.D. Thesis, Institut für Kernphysik, Technische Hochschule Darmstadt, Germany (1991).
- [41] R. Pedrys, D.J. Oostra, R.A. Haring, L. Calcagno, A. Haring and A.E. deVries, *Nucl. Instr. and Meth. B17* (1986) 15.
- [42] R.L. Fleischer, P. Price and R. Walker, *Nuclear Tracks in Solids* (Univ. of Calif. Press, Berkeley, CA, 1975).
- [43] G. Saeve, P. Hakansson, B. Sundqvist, E. Soderstroem, S.E. Lindqvist and J. Berg, *Int. J. Mass Spectrom. Ion Process.* 78 (1987) 259.
- [44] G. Schiwietz, P. Grande, B. Skogvall, R.K. J.P. Biersack, K. Sommer, A. Schmoldt, P. Goppelt, I. Kádár, S. Ricz and U. Stettner, *Phys. Rev. Lett.* 69/4 (1992) 628.
- [45] R. Schmidt, D. Brandl, C. Schoppmann, H. Voit, T. Kröhl, O. Johannsmann and W. Knoll, *Int. J. Mass Spectrom. Ion Process.* 99 (1990) 223.
- [46] J. Schou, *Nucl. Instr. and Meth. B27* (1987) 188.
- [47] A. Spieth, M.S. Thesis, Institut für Kernphysik, Technische Hochschule Darmstadt, Germany (1993).
- [48] B. Sundqvist, *Sputtering by Particle Bombardment*, vol. III (Springer, Berlin, 1992).
- [49] B.U.R. Sundqvist, *Int. J. Mass Spectrom. Ion Process.* 125 (1993) to be published.
- [50] T. Tonuma, H. Kumagai, T. Matsuo, H. Shibata and H. Tawara, *Nucl. Instr. and Meth. B67* (1992) 544.
- [51] D.F. Torgerson and R.P. Skowronski, *Biochem. Biophys. Res. Comm.* 60 (1974) 616.
- [52] Z. Vager, H. Feldmann, D. Kella, E. Malkin, E. Miklazky, J. Zajfman and R. Naaman, *Z. Phys. D19* (1991) 413.
- [53] C.C. Watson and T.A. Tombrello, *Radiat. Eff.* 89 (1985) 26.
- [54] W. Weltner and R.J.V. Zee, *Chem. Rev.* 89 (1989) 1713.
- [55] K. Wien, in: *Methods and Mechanisms for Producing Ions from Large Molecules*, vol. 269 of NATO ASI Science Series B, Minaki, Canada, 1990, eds. K.G. Standing and W. Ens (1991) p. 27.
- [56] K. Wien, O. Becker, W. Guthier, S.D. Negra, Y. LeBeyec, B. Monart, K. Standing, G. Maynard and G. Deutsch, *Int. J. Mass Spectrom. Ion Process.* 78 (1987) 273.